Stability analysis of the inverse Lax-Wendroff boundary treatment for high order upwind-biased finite difference schemes

Tingting Li[1], Chi-Wang Shu[2] and Mengping Zhang[3]

Abstract

In this paper, we consider linear stability issues for one-dimensional hyperbolic conservation laws using a class of conservative high order upwind-biased finite difference schemes, which is a prototype for the weighted essentially non-oscillatory (WENO) schemes, for initial-boundary value problems (IBVP). The inflow boundary is treated by the so-called inverse Lax-Wendroff (ILW) or simplified inverse Lax-Wendroff (SILW) procedure, and the outflow boundary is treated by the classical high order extrapolation. A third order total variation diminishing (TVD) Runge-Kutta time discretization is used in the fully discrete case. Both GKS (Gustafsson, Kreiss and Sundström) and eigenvalue analysis are performed for both semi-discrete and fully discrete schemes. The two different analysis techniques yield consistent results. Numerical tests are performed to demonstrate the stability results predicted by the analysis.

Key Words: high order upwind-biased schemes; inverse Lax-Wendroff procedure; simplified inverse Lax-Wendroff procedure; extrapolation; stability; GKS theory; eigenvalue analysis.

[1]School of Mathematical Sciences, University of Science and Technology of China, Hefei, Anhui 230026, P.R. China. E-mail: ltt1120@mail.ustc.edu.cn

[2]Division of Applied Mathematics, Brown University, Providence, RI 02912, USA. E-mail: shu@dam.brown.edu. Research supported by AFOSR grant F49550-12-1-0399 and NSF grant DMS-1418750.

[3]School of Mathematical Sciences, University of Science and Technology of China, Hefei, Anhui 230026, P.R. China. E-mail: mpzhang@ustc.edu.cn. Research supported by NSFC grant 11471305.

1 Introduction

When a high order finite difference scheme with wide stencil is used to solve hyperbolic conservation laws, the inner schemes cannot be used near the boundary. Special treatments near the boundaries are needed in order to maintain accuracy and stability. There exist two difficulties when imposing numerical boundary conditions. Firstly, the points used in these schemes which lie outside the computational domain, namely the "ghost points", should be evaluated properly. Secondly, the grid points may not coincide with the physical boundary exactly. For hyperbolic conservation laws, classical Lagrangian extrapolation to evaluate ghost point values near the outflow boundary usually leads to stable approximations. However, it is a challenge to obtain stable and accurate numerical boundary conditions near the inflow boundary. This is especially the case when the physical boundary does not coincide with but is very close to the first grid point, which is referred to as the "cut-cell" problem in the literature, see e.g. [2]. The inverse Lax-Wendroff (ILW) procedure, first introduced in [16], can overcome this difficulty. The simplified ILW (SILW) procedure, which is an extension of the ILW procedure and can save in algorithm complexity and computational cost, is introduced in [18]. For earlier related work, see [5, 6, 9, 8, 10].

Stability of the numerical schemes for initial boundary value problems (IBVP) on finite domain can be established by the normal mode analysis, which is based on the Laplace transform. General stability analysis based on this technique is the famous Gustafsson, Kreiss and Sundström (GKS) theory [7]. In [7], stability of fully discrete finite difference schemes is analyzed. In [15], stability analysis is performed for the semi-discrete cases. For the ILW and SILW procedures when high order central compact spatial operations are used, such GKS analysis has been performed in [19]. However, the GKS analysis may lead to high algebraic complexity in the case of very high order accuracy. An alternative technique, by visualizing the eigenvalue spectrum of the discretization operators, has also been used in [19] to analyze stability. It has been

observed in [19] that, when both techniques are used, they produce consistent stability conclusions. In this paper, we are interested in studying stability of semi-discrete and fully discrete upwind-biased high order finite difference schemes, which serve as a prototype for the weighted essentially non-oscillatory (WENO) schemes [12, 11, 13]. ILW and SILW procedures will be used near the inflow boundary and classical Lagrangian extrapolation will be used near the outflow boundary. Both the GKS analysis and the eigenvalue analysis will be performed.

This paper is organized as follows. In Section 2, we review high order upwind-biased finite difference methods as the inner schemes, and the third order total variation diminishing (TVD) Runge-Kutta time discretization method used in the full discretization. The ILW procedure, the SILW procedure and classical extrapolation are introduced in detail also in this section. Stability analysis is performed in Section 3 by using the GKS theory and the eigenvalue spectrum method, first for the semi-discrete case and then for the fully discrete case. Numerical tests are provided in Section 4 to demonstrate the results of the analysis. Concluding remarks are given in Section 5.

2 Scheme formulation

In this section, we review high order upwind-biased finite difference methods as the inner schemes, and the third order total variation diminishing (TVD) Runge-Kutta time discretization method used in the full discretization. We also introduce the ILW procedure, the SILW procedure and classical extrapolation used in the inflow and outflow boundary treatments.

2.1 High order upwind-biased finite difference schemes

Consider the one-dimensional scalar conservation law

$$\begin{cases} u_t + f(u)_x = 0, \ x \in [a,b], \ t \geq 0 \\ u(a,t) = g(t), \ t \geq 0 \\ u(x,0) = u_0(x), \ x \in [a,b] \end{cases} \tag{2.1}$$

Assume that $f'(u(a,t)) > 0$ and $f'(u(b,t)) > 0$ for $t > 0$. This assumption guarantees that the left boundary $x = a$ is an inflow boundary where a boundary condition is needed, and the right boundary $x = b$ is an outflow boundary where no boundary condition can be prescribed.

The interval (a, b) is discretized by an uniform mesh as

$$a + C_a\ \Delta x = x_0 < x_1 < x_2 < \cdots < x_N = b - C_b\ \Delta x \tag{2.2}$$

where $C_a \in [0, 1)$ and $C_b \in [0, 1)$. $\{x_j = a + (C_a + j)\ \Delta x,\ j = 0, 1, 2, \cdots N\}$ are the grid points. The first and the last grid points are not necessarily aligned with the boundary, and we choose this kind of discretization on purpose.

The general semi-discrete conservative finite difference scheme approximating (2.1), based on point values and numerical fluxes, is of the form:

$$\frac{du_j}{dt} = -\frac{1}{\Delta x}\ (\hat{f}_{j+\frac{1}{2}}(t) - \hat{f}_{j-\frac{1}{2}}(t)) \tag{2.3}$$

where the numerical flux $\hat{f}_{j+\frac{1}{2}}$ is defined as a linear combination of $f(u(x,t))$ in the neighborhood of x_j such that the right hand of (2.3) approximates $-f(u)_x$ at $x = x_j$ to the desired order of accuracy.

For convenience, the semi-discrete approximation (2.3) can be written as

$$\frac{du_j}{dt} = -\frac{1}{\Delta x}\mathcal{D}_{j,\hat{k},\hat{m}} \cdot f_j \equiv -\frac{1}{\Delta x}\sum_{l=0}^{\hat{m}} d_{\hat{k},l}\ f_{j-\hat{k}+l} \tag{2.4}$$

where $j - \hat{k}$ denotes the left most point of the derivative stencil having $\hat{m} + 1$ points. Both $\hat{k}$ and $\hat{m}$ depend on the order of the scheme.

Schemes considered in this paper are listed below.

- Third order scheme

$$\frac{du_j}{dt} = -\frac{1}{\Delta x}\ (\frac{1}{6}f_{j-2} - f_{j-1} + \frac{1}{2}f_j + \frac{1}{3}f_{j+1})$$

- Fifth order scheme

$$\frac{du_j}{dt} = -\frac{1}{\Delta x}\ (-\frac{1}{30}f_{j-3} + \frac{1}{4}f_{j-2} - f_{j-1} + \frac{1}{3}f_j + \frac{1}{2}f_{j+1} - \frac{1}{20}f_{j+2})$$

- Seventh order scheme

$$\frac{du_j}{dt} = -\frac{1}{\Delta x}\,(\frac{1}{140}f_{j-4} - \frac{7}{105}f_{j-3} + \frac{3}{10}f_{j-2} - f_{j-1} + \frac{1}{4}f_j + \frac{3}{5}f_{j+1} - \frac{1}{10}f_{j+2} + \frac{1}{105}f_{j+3})$$

- Ninth order scheme

$$\frac{du_j}{dt} = -\frac{1}{\Delta x}\,(-\frac{1}{630}f_{j-5} + \frac{1}{56}f_{j-4} - \frac{2}{21}f_{j-3} + \frac{1}{3}f_{j-2} - f_{j-1} + \frac{1}{5}f_j + \frac{2}{3}f_{j+1} - \frac{1}{7}f_{j+2} + \frac{1}{42}f_{j+3} - \frac{1}{504}f_{j+4})$$

- Eleventh order scheme

$$\frac{du_j}{dt} = -\frac{1}{\Delta x}\,(\frac{1}{2772}f_{j-6} - \frac{1}{210}f_{j-5} + \frac{5}{168}f_{j-4} - \frac{5}{42}f_{j-3} + \frac{5}{14}f_{j-2} - f_{j-1} + \frac{1}{6}f_j + \frac{5}{7}f_{j+1} - \frac{5}{28}f_{j+2} + \frac{5}{126}f_{j+3} - \frac{1}{168}f_{j+4} + \frac{1}{2310}f_{j+5})$$

- Thirteenth order scheme

$$\frac{du_j}{dt} = -\frac{1}{\Delta x}\,(-\frac{1}{12012}f_{j-7} + \frac{1}{792}f_{j-6} - \frac{1}{110}f_{j-5} + \frac{1}{24}f_{j-4} - \frac{5}{36}f_{j-3} + \frac{3}{8}f_{j-2} - f_{j-1} + \frac{1}{7}f_j + \frac{3}{4}f_{j+1} - \frac{5}{24}f_{j+2} + \frac{1}{18}f_{j+3} - \frac{1}{88}f_{j+4} + \frac{1}{660}f_{j+5} - \frac{1}{10296}f_{j+6})$$

Notice that all schemes have one more point on the left than on the right for their stencils, considering the positive wind direction. This is why the schemes are called "upwind-biased". Also notice that these schemes are just the standard WENO schemes with the linear weights (when the smoothness indicators and nonlinear weights are turned off), see [1].

2.2 Time discretization

We use a third order TVD Runge-Kutta method [14] to integrate the semi-discrete system of ordinary differential equations (ODEs) (2.3) in time. For simplicity, the system of the initial value problems of ODEs is written as

$$u_t = \mathcal{L}u$$

From the time level t_n to t_{n+1}, the third order TVD Runge-Kutta method is given by

$$\begin{aligned} u^{(1)} &= u^n + \Delta t \mathcal{L}(u^n) \\ u^{(2)} &= \frac{3}{4}u^n + \frac{1}{4}u^{(1)} + \frac{1}{4}\Delta t \mathcal{L}(u^{(1)}) \\ u^{n+1} &= \frac{1}{3}u^n + \frac{2}{3}u^{(2)} + \frac{2}{3}\Delta t \mathcal{L}(u^{(2)}) \end{aligned}$$

where Δt is the time step.

Special attention must be taken when we impose time dependent boundary conditions in the two interior stages of the Runge-Kutta method. With the time dependent boundary condition $g(t)$, the traditional match of time is

$$\begin{aligned} u^n &\sim g(t_n) \\ u^{(1)} &\sim g(t_n + \Delta t) \\ u^{(2)} &\sim g(t_n + \frac{\Delta t}{2}) \end{aligned}$$

but this would decrease the accuracy to second order as pointed out in [3]. So we use the following match of time which is analyzed in [3] to ensure third order accuracy in the time discretization

$$\begin{aligned} u^n &\sim g(t_n) \\ u^{(1)} &\sim g(t_n) + \Delta t g'(t_n) \\ u^{(2)} &\sim g(t_n) + \frac{1}{2}\Delta t g'(t_n) + \frac{1}{4}\Delta t^2 g''(t_n) \end{aligned}$$

2.3 The inverse Lax-Wendroff (ILW) procedure

The basic idea of the ILW procedure is to use Taylor expansion at the boundary point and then repeatedly use the PDE and its time derivatives to convert spatial derivatives to time derivatives, in order to obtain accurate values at the relevant ghost points. The procedure is summarized as follows.

A Taylor expansion at the boundary point a gives

$$u(x_{-p}) = u(a + (C_a - p)\Delta x) = \sum_{k=0}^{d-1} \frac{u^{*(k)}(\Delta x)^k(-p + C_a)^k}{k!} + \mathcal{O}(\Delta x^d)$$

where $u(x_{-p})$ is the value of the function u at the ghost point x_{-p}. Clearly,

$$u_{-p} = \sum_{k=0}^{d-1} \frac{u^{*(k)}(\Delta x)^k(-p+C_a)^k}{k!} \tag{2.5}$$

is a d-th order approximation of $u(x_{-p})$, if $u^{*(k)}$ is an (at least) $(d-k)$-th order approximation of $\frac{\partial^k u}{\partial x^k}|_{x=a}$. For the ILW procedure, the values of $u^{*(k)}$ can be obtained as follows

$$\begin{aligned}
u^{*(0)} &= u(a,t) = g(t) \\
u^{*(1)} &= \frac{\partial u}{\partial x}|_{x=a} = -\frac{g'(t)}{f'(g(t))} \\
u^{*(2)} &= \frac{\partial^2 u}{\partial x^2}|_{x=a} = \frac{f'(g(t))g''(t) - 2f''(g(t))(g'(t))^2}{(f'(g(t)))^3} \\
u^{*(3)} &= \frac{\partial^3 u}{\partial x^3}|_{x=a} \\
&= \frac{9f'(g(t))f''(g(t))g'(t)g''(t) + 3f'(g(t))f'''(g(t))(g'(t))^3}{(f'(g(t)))^5} \\
&\quad + \frac{-(f'(g(t)))^2 g'''(t) - 12(f''(g(t)))^2(g'(t))^3}{(f'(g(t)))^5} \\
&\cdots
\end{aligned}$$

In this way, we can get $u^{*(k)},\ k = 0, 1, 2 \cdots d-1$, through the given boundary data $g(t)$ and its time derivatives. Plugging them into (2.5), we can obtain u_{-p}.

2.4 The simplified inverse Lax-Wendroff (SILW) procedure

The ILW procedure outlined in the previous subsection can be easily verified for stability through the GKS theory, both for the semi-discrete version [16] and for the fully discrete version. However, for multi-dimensional nonlinear PDE systems, the derivation of $u^{*(k)}$ through the ILW procedure can be algebraically very complicated. This is especially the case for problems with moving boundaries [17]. A simplified version of the ILW procedure, which is referred to as SILW, is introduced in [18] to save in algorithm complexity and computational cost. This SILW procedure is analyzed for its stability in [19] for spatially central compact discretizations.

The SILW procedure also uses (2.5) to obtain u_{-p}. For $k \le k_d - 1$, $u^{*(k)}$ is obtained in the same way as in the ILW procedure. For $k \ge k_d$, $u^{*(k)}$ is obtained by the classical Lagrangian extrapolation as $u^{*(k)} = \frac{\partial^k P_d}{\partial x^k}|_{x=a}$, where $P_d(x)$ is an interpolation polynomial of order d using points inside the computational domain. We refer to the next subsection for the details of the construction of $P_d(x)$. Clearly, the choice of the threshold index k_d will be a key issue to ensure stability, which will be discussed in detail later in this paper.

It would appear that it might benefit to use the partial information of $u^{*(k)}$ for $k \le k_d - 1$, which are obtained through the ILW procedure using the given boundary data $g(t)$ and its derivatives, when constructing the polynomial $P_d(x)$, so that fewer points inside the computational domain need to be used. However, it turns out that this would make the scheme less stable [19]. Therefore, in this paper we consider only the pure interpolation polynomial $P_d(x)$ without using the boundary data $g(t)$, for computing $u^{*(k)}$ with $k \ge k_d$.

2.5 Extrapolation

In order to obtain u_{N+p} for the ghost points near the outflow boundary, we use the d points inside the computational domain, $\{(x_N, u_N),\ (x_{N-1}, u_{N-1}), \cdots,\ (x_{N-d+1}, u_{N-d+1})\}$ to obtain a classical interpolation polynomial $P_d(x)$ of degree $d-1$, and then take $u_{N+p} = P_d(x_{N+p})$ to approximate $u(x_{N+p})$ with is accurate of order d. That is,

$$u_{N+p} = \sum_{i=1}^{d} \beta_i\ u_{N+1-i}$$

where $\{\beta_i, i = 1, 2, \cdots, d\}$ are the coefficients defined by

$$\beta_i = \prod_{t=1, t\neq i}^{d} \frac{t+p-1}{t-i}$$

The complete scheme of the numerical approximation to the one-dimensional scalar conservation law (2.1) is as follows. One of the schemes in Section 2.1 is used as the inner scheme, which is used everywhere inside the computational domain. The necessary ghost

point values are obtained as below. Ghost point values of u near the inflow boundary are obtained by the ILW procedure or the SILW procedure introduced in Section 2.3 and Section 2.4 respectively, and ghost point values of u near the outflow boundary are obtained by extrapolation introduced in Section 2.5. The third order TVD Runge-Kutta method introduced in Section 2.2 is used as the time discretization. Of course, the specific third order TVD Runge-Kutta method is used here only as an example, and other time discretization methods can also be used.

3 Stability analysis

Stability analysis for the semi-discrete schemes and the fully discrete schemes are discussed in this section. Both GKS and eigenvalue spectrum visualization methods are used. Here, the analysis is performed on the one-dimensional linear IBVP (2.1) corresponding to $f(u) = cu$ with $c > 0$ and the third order TVD Runge-Kutta scheme.

3.1 The semi-discrete schemes

In this subsection we discuss semi-discrete schemes.

3.1.1 The GKS analysis

The procedure of the GKS analysis for the semi-discrete schemes is:

(1) Divide the problem into the summation of three simpler problems: one Cauchy problem on $(-\infty, +\infty)$ and two quarter-plane problems on the domains $[a, +\infty)$ and $(-\infty, b]$, respectively.

(2) For the Cauchy problem, stability can be obtained by standard Fourier analysis. The following analysis is performed under the assumption that the inner scheme corresponding to the Cauchy problem is stable.

(3) For a quarter-plane problem, a necessary and sufficient condition for stability is that there exists no eigensolution (to be explained later).

Take $u_j(t) = e^{st}\phi_j$, (2.4) becomes

$$\Delta x s\phi_j + c(\mathcal{D}_{j,\hat{k},\hat{m}} \cdot \phi_j) = 0 \tag{3.6}$$

$\{\phi_j(s)\}_0^\infty$ is an eigensolution if it satisfies the following constraints:

(1) It is not identically 0.

(2) It satisfies (3.6) at all points where it is applied and the numerical boundary conditions.

(3) $Re(s) \geq 0$.

(4) For $Re(s) > 0$, the corresponding solution satisfies (1) and (2) and

$$\lim_{j\to\infty} \phi_j(s) = 0 \tag{3.7}$$

(5) For $Re(s) = 0$, the corresponding solution should satisfy (1), (2) and (4) with respect to s_0 where

$$s_0 = \lim_{\epsilon\to 0^+} (s + \varepsilon)$$

Here, ε is a real and small positive perturbation.

Functions satisfying the corresponding constrains above with $Re(s) < 0$ can also be regarded as an eigensolution. But the definition here is just made on those eigensolutions which are interesting for the stability analysis.

s is regarded as an eigenvalue and the corresponding $\{\phi_j(s)\}_0^\infty$ as an eigensolution. If an eigenvalue and the associated eigensolution exist, the scheme is unstable. Otherwise, the scheme is stable.

Firstly, stability analysis is performed on the right-quarter plane problem:

$$\begin{cases} u_t + c\ u_x = 0,\ x \in [a, +\infty],\ t \geq 0,\ c > 0 \\ u(a,t) = g(t),\ t \geq 0 \\ u(x,0) = u_0(x),\ x \in [a, +\infty] \end{cases} \tag{3.8}$$

For the purpose of stability analysis, $g(t)$ can be set to zero without loss of generality.

We take first the third order inner scheme to approximate (3.8), which can be written as

$$\frac{du_j}{dt} = -\frac{c}{\Delta x}(\frac{1}{6}u_{j-2} - u_{j-1} + \frac{1}{2}u_j + \frac{1}{3}u_{j+1}), \quad j = 2, 3, \cdots \tag{3.9}$$

Let $u_j = e^{st}\phi_j$, (3.9) can be transformed into

$$\tilde{s}\phi_j = -(\frac{1}{6}\phi_{j-2} - \phi_{j-1} + \frac{1}{2}\phi_j + \frac{1}{3}\phi_{j+1}) \tag{3.10}$$

Here $\tilde{s} = s\frac{\Delta x}{c}$. $\tilde{s}$ can also be regarded as the eigenvalue and $\{\phi_j(\tilde{s})\}_0^\infty$ is the corresponding eigensolution.

The characteristic equation is obtained by taking $\phi_j = \kappa^j$ in (3.10):

$$\tilde{s}\kappa^2 = -(\frac{1}{6} - \kappa + \frac{1}{2}\kappa^2 + \frac{1}{3}\kappa^3) \tag{3.11}$$

Let

$$q(\kappa) = \tilde{s}\kappa^2 + (\frac{1}{6} - \kappa + \frac{1}{2}\kappa^2 + \frac{1}{3}\kappa^3)$$

Take $\kappa = e^{\imath\xi}$, $\xi \in [0, 2\pi]$. This means $|\kappa| = 1$. From (3.11), we can get

$$\tilde{s} = -\frac{1}{6}e^{-2\imath\xi} + e^{-\imath\xi} - \frac{1}{2} - \frac{1}{3}e^{\imath\xi}$$

Figure 3.1 shows the locus of $\tilde{s}$ for $|\kappa| = 1$ ($\xi \in [0, 2\pi]$).

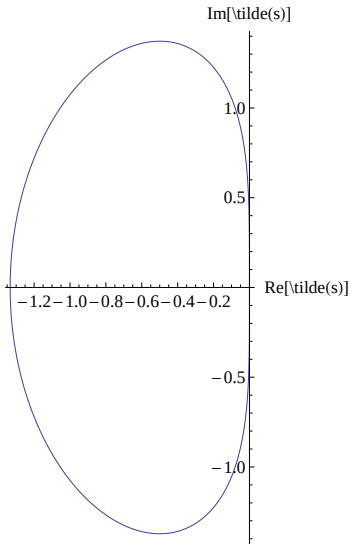

Figure 3.1: Locus of $\tilde{s}$

Figure 3.1 shows that, if $|\kappa| = 1$, $Re(\tilde{s}) \leq 0$.

Since the domain here is $[a, +\infty)$, the limit in (3.7) is $j \to +\infty$. We are only interested in the roots of the characteristic equation which satisfy $|\kappa| < 1$.

If $Re(\tilde{s}) > 0$, Figure 3.1 shows that the roots of Equation (3.11) would satisfy $|\kappa| \neq 1$, since the locus of $\tilde{s}$ for $|\kappa| = 1$ does not come to the right half plane. If there exist s_1 and s_2 both on the right half plane (namely $Re(\tilde{s_1}) > 0$ and $Re(\tilde{s_2}) > 0$), such that the number of roots with $|\kappa| < 1$ for $\tilde{s} = s_1$ is different from and larger than the number of roots with $|\kappa| < 1$ for $\tilde{s} = s_2$, then there must be a root which changes from $|\kappa_1(\tilde{s_1})| > 1$ to $|\kappa_1(\tilde{s_2})| < 1$. As the roots are continuous functions of the coefficient $\tilde{s}$, there must be a $\tilde{s_3}$ with $Re(\tilde{s_3}) > 0$ such that the root satisfies $|\kappa_1(\tilde{s_3})| = 1$. This is in contradiction with the result of Figure 3.1. In conclusion, if $Re(\tilde{s}) > 0$, the number of roots with $|\kappa| < 1$ of the characteristic equation is independent of $\tilde{s}$. One can choose any $\tilde{s}$ which satisfies $Re(\tilde{s}) > 0$ to get the number of roots with $|\kappa| < 1$. Taking $\tilde{s} = 1$, the roots of (3.11) are

$$\kappa_1 = 0.303322 + 0.076861\imath,\ \kappa_2 = 0.303322 - 0.076861\imath,\ \kappa_3 = -5.10664$$

So, if $Re(\tilde{s}) > 0$, there are two roots satisfying $|\kappa| < 1$.

If $Re(\tilde{s}) = 0$, $\tilde{s} = h\imath$. One can find that (i) $h \in [0, h_{max}]$ (here h_{max} is about 0.1), the three roots of the characteristic equation satisfy $|\kappa_1| = 1$, $|\kappa_2| < 1$, $|\kappa_3| > 1$. (ii) $h \in [h_{max}, +\infty)$, the three roots satisfy $|\kappa_1| < 1$, $|\kappa_2| < 1$ and $|\kappa_3| > 1$.

If $|\kappa_1| = 1$, a perturbation analysis is used to decide whether the scheme is stable. For instance, the roots of the characteristic equation with $\tilde{s} = 0$ are $\kappa_1 = 1$, $\kappa_2 = \frac{1}{4}(-5 + \sqrt{33})$, $\kappa_3 = \frac{1}{4}(-5 - \sqrt{33})$. We have to determine whether $\kappa_1 = 1$ is stable to perturbation or not. To do so, we substitute $\tilde{s} = \delta$ and $\kappa = 1+\epsilon$ into the the characteristic equation (3.11) and obtain $\delta = -(1/6 - (1 + \epsilon) + (1 + \epsilon)^2/2 + (1 + \epsilon)^3/3)/(1 + \epsilon)^2$. Taylor expansion at $\epsilon = 0$ gives $\delta = -\epsilon + O(\epsilon^2)$. If $\delta > 0$ which indicates $Re(\tilde{s}) > 0$, $|\kappa| = |1 + \epsilon| < 1$. $\kappa = 1$ is thus stable under perturbation.

In conclusion, for any value of $\tilde{s}$ satisfying $Re(\tilde{s}) \geq 0$, the roots of the characteristic equation satisfy $|\kappa_1| \leq 1,\ |\kappa_2| < 1,\ |\kappa_3| > 1$ and $\kappa_1 = 1$ is stable under perturbation.

Case 1. If κ_1 and κ_2 are distinct, the general expression of ϕ_j is:

$$\phi_j = \sigma_1 \kappa_1^j + \sigma_2 \kappa_2^j \tag{3.12}$$

$\sigma_1,\ \sigma_2$ are two constants which remain to be determined by the numerical boundary conditions.

For the ILW boundary condition, the numerical boundary conditions are (3.10) with $j = 0,\ 1$ with the values of the ghost points obtained through the ILW procedure. As $g(t) = 0,\ u_{-1} = 0,\ u_{-2} = 0$ and $\phi_{-1} = 0,\ \phi_{-2} = 0$. The numerical boundary conditions become:

$$\begin{aligned} \tilde{s}\phi_0 &= -(\frac{1}{2}\phi_0 + \frac{1}{3}\phi_1) \\ \tilde{s}\phi_1 &= -(-\phi_0 + \frac{1}{2}\phi_1 + \frac{1}{3}\phi_2) \end{aligned} \tag{3.13}$$

Putting (3.12) into (3.13), one can get a linear system $A\sigma = 0$ with $\sigma = (\sigma_1,\ \sigma_2)^T$. The coefficient matrix is

$$A = \begin{pmatrix} \tilde{s} + \frac{1}{2} + \frac{1}{3}\kappa_1 & \tilde{s} + \frac{1}{2} + \frac{1}{3}\kappa_2 \\ -1 + (\tilde{s} + \frac{1}{2})\kappa_1 + \frac{1}{3}\kappa_1^2 & -1 + (\tilde{s} + \frac{1}{2})\kappa_2 + \frac{1}{3}\kappa_2^2 \end{pmatrix}$$

In order to get nontrivial ϕ_j, σ_1 and σ_2 cannot be equal to zero at the same time. The determinant of the matrix A then must equal to 0. $\{\tilde{s},\ \kappa_1,\ \kappa_2\}$ are obtained by $\{q(\kappa_1) = 0,\ q(\kappa_2) = 0,\ det(A) = 0,\ \kappa_1 \neq \kappa_2\}$. The system has no solution.

Case 2. If $\kappa_1 = \kappa_2 = \kappa$, the general expression of ϕ_j is:

$$\phi_j = \sigma_1 \kappa^j + \sigma_2 j \kappa^j \tag{3.14}$$

The numerical boundary conditions are (3.13). Putting (3.14) into (3.13), one can get a linear system $A\sigma = 0$. The coefficient matrix is

$$A = \begin{pmatrix} \tilde{s} + \frac{1}{2} + \frac{1}{3}\kappa & \frac{1}{3}\kappa \\ -1 + (\tilde{s} + \frac{1}{2})\kappa + \frac{1}{3}\kappa^2 & (\tilde{s} + \frac{1}{2})\kappa + \frac{2}{3}\kappa^2 \end{pmatrix}$$

here κ is a multiple root of the equation $q(\kappa)=0$ and it satisfies $\{q(\kappa)=0,\ q^{'}(\kappa)=0\}$. Solving this system, one can get the roots:

$$\{\tilde{s}=0.890809,\ \kappa=0.322185\},\ \{\tilde{s}=-0.445405-1.15981\imath,\ \kappa=-0.161093+1.75438\imath\},$$

$$\{\tilde{s}=-0.445405+1.15981\imath,\ \kappa=-0.161093-1.75438\imath\}$$

The root satisfying $Re(\tilde{s})>0$ and $|\kappa|<1$ is $\{\tilde{s}=0.890809,\ \kappa=0.322185\}$. Putting it into $A\sigma=0$, we obtain $det(A)=0.830576$ and $\{\sigma_1=0,\ \sigma_2=0\}$. Thus it is not an eigensolution.

In conclusion, the scheme (3.8) with the third order inner scheme and the ILW procedure boundary treatment has no eigensolution, hence it is stable. In fact, since the ghost point values are completely determined by the boundary data $g(t)$ and its derivatives and do not depend on the numerical solution inside the computational domain, when $g(t)=0$ all the ghost point values are zero. Hence stability of the IBVP for the scheme is the same as that for the inner scheme without boundary. That is, stability for the ILW boundary condition is the same as that for the Cauchy problem of the inner scheme [16].

Next, we use the SILW procedure to obtain values of ghost points and repeat the previous analysis. In this case, the values of $u_{-1},\ u_{-2}$ are functions of C_a and they change with different choices of k_d. Hence, the coefficient matrix of the linear system for $\{\sigma_1,\ \sigma_2\}$ is a function of C_a and changes with k_d, too. If $k_d=1$, derivatives at the boundary point $x=a$ are:

$$\begin{aligned}
u^{*(0)} &= 0\\
u^{*(1)} &= -\frac{(3+2C_a)u_0-4(1+C_a)u_1+(1+2C_a)u_2}{2\Delta x}\\
u^{*(2)} &= \frac{u_0-2u_1+u_2}{(\Delta x)^2}
\end{aligned}$$

Putting this into (2.5), we obtain

$$\begin{aligned}
\phi_{-1} &= (-\frac{C_a^2}{2}-\frac{3}{2}C_a+2)\phi_0+(C_a^2+2C_a-3)\phi_1+(-\frac{C_a^2}{2}-\frac{C_a}{2}+1)\phi_2\\
\phi_{-2} &= (-\frac{C_a^2}{2}-\frac{3}{2}C_a+5)\phi_0+(C_a^2+2C_a-8)\phi_1+(-\frac{C_a^2}{2}-\frac{C_a}{2}+3)\phi_2
\end{aligned} \tag{3.15}$$

The numerical boundary conditions are

$$\begin{aligned}
&\frac{1}{12}(-8+15C_a+5C_a^2+12\tilde{s})\phi_0+\frac{1}{6}(12-10C_a-5C_a^2)\phi_1+\frac{1}{12}(-6+5C_a+5C_a^2)\phi_2=0\\
&\frac{1}{12}(-8-3C_a-C_a^2)\phi_0+\frac{1}{12}(4C_a+2C_a^2+12\tilde{s})\phi_1+\frac{1}{12}(6-C_a-C_a^2)\phi_2=0
\end{aligned} \tag{3.16}$$

The characteristic equation is (3.11).

Case 1. If κ_1 and κ_2 are different. ϕ_j is in the form (3.12). Putting it into (3.16), we can get a linear system $A\sigma=0$ for $\{\sigma_1,\ \sigma_2\}$ with the coefficient matrix

$$A=\begin{pmatrix} f_1(\kappa_1) & f_1(\kappa_2)\\ f_2(\kappa_1) & f_2(\kappa_2)\end{pmatrix}$$

where

$$\begin{aligned}
f_1(\kappa)&=-\frac{2}{3}+\frac{5}{12}C_a^2(\kappa-1)^2+2\kappa-\frac{1}{2}\kappa^2+\frac{5}{12}C_a(3-4\kappa+\kappa^2)+\tilde{s}\\
f_2(\kappa)&=-\frac{2}{3}-\frac{1}{12}C_a^2(\kappa-1)^2+\frac{1}{2}\kappa^2-\frac{1}{12}C_a(3-4\kappa+\kappa^2)+\kappa\tilde{s}
\end{aligned}$$

We can solve $\{det(A)=0,\ q(\kappa_1)=0,\ q(\kappa_2)=0,\ |\kappa_1|<1,\ |\kappa_2|<1,\ \kappa_1\neq\kappa_2\}$ to get $\tilde{s},\ \kappa_1,\ \kappa_2$ for different values of C_a. There may exist more than one eigenvalue $\tilde{s}$ and we compute the largest real part of all the eigenvalues. By using the software Mathematica we get the result as in Figure 3.2.

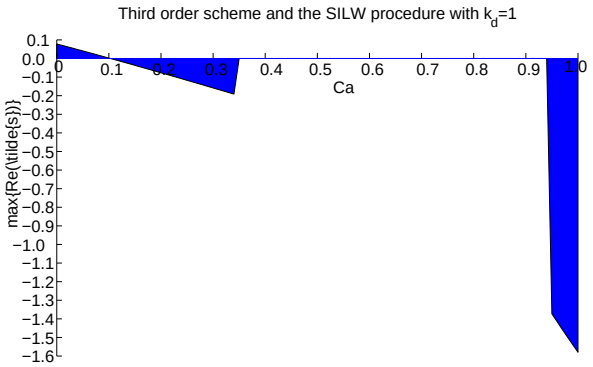

Figure 3.2: GKS analysis for the third order scheme and the SILW procedure with $k_d=1$

From Figure 3.2, we can find that for small values of C_a (which correspond to the situation that the boundary does not coincide with but is very close to the first grid

point, a typical case in "cut cells"), there exist non-trivial solutions of $Re(\tilde{s}) > 0$. The third order scheme and the SILW procedure with $k_d = 1$ is thus not stable for all values of C_a.

Case 2. If $\kappa_1 = \kappa_2 = \kappa$, ϕ_j is in the form (3.14). In this case, the numerical boundary conditions are (3.16) and the linear system $A\sigma = 0$ for $\{\sigma_1,\ \sigma_2\}$ has the coefficient matrix

$$A = \begin{pmatrix} a_{11} & a_{12} \\ \\ a_{21} & a_{22} \end{pmatrix}$$

where

$$\begin{aligned}
a_{11} &= -\frac{2}{3} + \frac{5}{12}C_a^2(\kappa-1)^2 + 2\kappa - \frac{1}{2}\kappa^2 + \frac{5}{12}C_a(\kappa^2 - 4\kappa + 3) + \tilde{s} \\
a_{12} &= -\kappa(\kappa-2) + \frac{5}{6}C_a\kappa(\kappa-2) + \frac{5}{6}C_a^2\kappa(\kappa-1) \\
a_{21} &= -\frac{2}{3} - \frac{1}{12}C_a^2(\kappa-1)^2 + \frac{1}{2}\kappa^2 - \frac{1}{12}C_a(3 - 4\kappa + \kappa^2) + \kappa\tilde{s} \\
a_{22} &= -\frac{1}{6}C_a\kappa(\kappa-2) - \frac{1}{6}C_a^2\kappa(\kappa-1) + \kappa(\kappa + \tilde{s})
\end{aligned}$$

As before, the relevant pair is $\{\tilde{s} = 0.890809,\ \kappa = 0.322185\}$. In order to obtain non-trivial eigensolutions, $det(A)$ should be zero. This leads to $C_a = -2.31192 - 1.49087\imath$ or $C_a = -2.31192 + 1.49087\imath$. Since C_a is a real number in $[0, 1)$, there has no eigensolution.

If we perform the same analysis as before with $k_d = 2$, we can find that there exists no nontrivial eigensolution for all values of C_a.

When we use the SILW procedure to obtain values of ghost points, we always expect to find $(k_d)_{\min}$, the minimum number of derivatives needed to be obtained through the ILW procedure, which can ensure stability for any position C_a. For the third order semi-discrete scheme, $(k_d)_{\min} = 2$.

Secondly, stability analysis is performed on the left-quarter plane problem

$$\begin{cases} u_t + c\ u_x = 0,\ x \in (-\infty, b],\ t \geq 0,\ c > 0 \\ \\ u(x,0) = u_0(x),\ x \in (-\infty, b] \end{cases} \tag{3.17}$$

For such outflow boundary, values of the ghost points are obtained by classical extrapolation, and they have no relationship with C_b. Similar GKS analysis as performed before

for the inflow case can be applied here. The characteristic equation is still (3.11). The eigensolution here is $\{\phi_j(s)\}_{-\infty}^{N}$, hence the condition (3.7) is replaced by

$$\lim_{j\to-\infty}\phi_j(s)=0$$

Now we should focus on the roots of (3.11) which satisfy $|\kappa|>1$. As before, there is one root which satisfies this property, so we can get $\phi_j=\sigma\kappa^j$. If the values of the ghost points are obtained by the third order extrapolation

$$u_{N+1}=u_{N-2}-3u_{N-1}+3u_N$$

the numerical boundary condition at $j=N$ is obtained

$$\tilde{s}\phi_N=-(\frac{1}{2}\phi_{N-2}-2\phi_{N-1}+\frac{3}{2}\phi_N)$$

By $\phi_j=\sigma\kappa^j$, we can see that the numerical boundary condition is

$$\sigma(\frac{1}{2}-2\kappa+(\tilde{s}+\frac{3}{2})\kappa^2)=0$$

In order to get nontrivial solution, that is, $\sigma\neq 0$, we need that

$$\begin{cases}\dfrac{1}{2}-2\kappa+(\tilde{s}+\dfrac{3}{2})\kappa^2=0\\ q(\kappa)=0\end{cases}$$

Solving this system, we can get $\{\tilde{s}=0,\ \kappa=1\}$. From the previous analysis, we already know that $\kappa=1$ will transform to $|\kappa|<1$ after perturbation, hence it is not an eigensolution. So, problem (3.17) with the third order scheme is stable.

In fact, it is proved in [4] that a stable finite difference scheme with outflow extrapolation is stable for a linear hyperbolic initial value problem.

3.1.2 Eigenvalue spectrum visualization

Unlike the GKS analysis, which considers the boundary conditions at each end separately, the method of eigenvalue spectrum visualization [19] considers stability with the

two boundaries together. Again, in the case of stability analysis, we set $g(t) = 0$ without loss of generality.

The semi-discrete schemes can be expressed as a linear system of equations in a matrix-vector form as

$$\frac{d\vec{U}}{dt} = -\frac{c}{\Delta x} Q\vec{U} \tag{3.18}$$

where $\vec{U} = (u_0,\ u_1,\ \cdots,\ u_n)^T$ and Q is the coefficient matrix of the spatial discretization. This system contains the chosen inner scheme as well as two numerical boundary conditions.

Let $u(x,t) = e^{st}v(x)$, (3.18) changes to

$$\tilde{s}\vec{U} = -Q\vec{U} \tag{3.19}$$

A nontrivial solution $\vec{U}$ satisfying (3.19) is an eigenvector of the matrix $-Q$ and $\tilde{s}$ is the corresponding eigenvalue. The problem reduces to finding whether there exists any eigenvalue of $-Q$ with $Re(\tilde{s}) > 0$. As pointed out in [19], we only need to focus on the eigenvalues which keep $O(1)$ distance from the imaginary axis when the grid number N increases. Just like in the GKS analysis, there may be more than one such eigenvalues of the matrix $-Q$, and we choose the largest real part of all the candidate eigenvalues. We perform this analysis with the third order scheme and the SILW procedure with $k_d = 1$ as an example, using the Matlab. The result is in Figure 3.3, in which we have used three different values of N ($N = 320$, 640 and $1,280$) and have observed that the largest real part of all the candidate eigenvalues (as plotted) is basically fixed when N changes over this range.

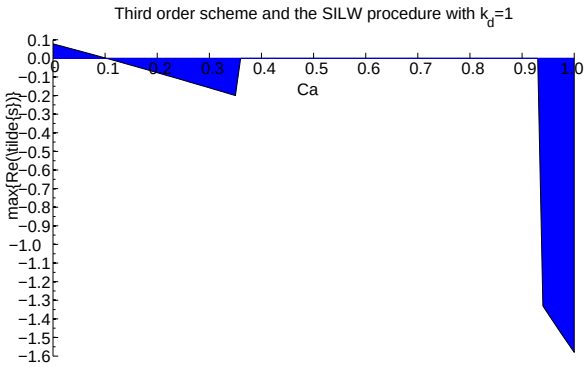

Figure 3.3: Eigenspectrum analysis: third order scheme and the SILW procedure with $k_d = 1$

Comparing Figure 3.2 and Figure 3.3, we find that they are almost the same. This gives us confidence that the eigenspectrum analysis can produce reliable conclusions about stability, even though it is less mathematically rigorous.

3.2 Fully-discrete schemes

In reality, we always use fully-discrete schemes to solve the problems. This includes time discretization of the semi-discrete scheme. In this paper, the third order TVD Runge-Kutta time discretization is used as an example. Firstly, we recall the stability domain of such time discretization method. Let us consider the following general system

$$\frac{du}{dt} = F(t, u)$$

To derive the stability domain, we use $F(t, u) = su$. This relationship substituted in the third order time discretization leads to the time discrete equation

$$u^{n+1} = (1 + \mu + \frac{\mu^2}{2} + \frac{\mu^3}{6})u^n$$

where $u^n = u(x, t_n)$, $\mu = s\Delta t$, and Δt is the time step. Assuming a solution is of the form $u^n = z^n u^0$, here z is a complex number, the stability domain of the method is

$$|z(\mu)| \leq 1, \ z(\mu) = 1 + \mu + \frac{\mu^2}{2} + \frac{\mu^3}{6} \tag{3.20}$$

Recall that, in the semi-discrete case, an eigensolution is in the form $u_j(t) = e^{st}\phi_j = e^{\tilde{s}c\frac{t}{\Delta x}}\phi_j$ with $Re(\tilde{s}) \geq 0$. In the fully-discrete scheme, an eigensolution is in the form $u_j^{n+1} = z(\mu)u_j^n$ with $\mu = \tilde{s}\frac{c\Delta t}{\Delta x}$ and $|z(\mu)| > 1$. Here $\tilde{s}$ is an eigenvalue of the semi-discrete scheme. In both semi-discrete and fully discrete cases, the scheme is unstable if such candidate eigensolution exists. Take

$$\lambda_{cfl} = \frac{c\Delta t}{\Delta x}$$

where $\lambda_{cfl} > 0$. From now on, we would like to verify stability with $(\lambda_{cfl})_{\max}$, which is the maximum value of λ_{cfl} to ensure stability for the corresponding Cauchy problem. In other words, we would not want the boundary condition to reduce the CFL number for stability.

In the periodic case, solutions can be assumed to be $u_j(t) = \frac{1}{\sqrt{2\pi}}\hat{u}(\omega, t)e^{\imath\omega x}$. In this circumstance, the third order scheme can be transformed to:

$$\begin{aligned}\frac{d\hat{u}(\omega,t)}{dt} &= \frac{c}{\Delta x}\hat{u}(\omega,t)(-\frac{1}{6}e^{-2\imath\omega\triangle x} + e^{-\imath\omega\triangle x} - \frac{1}{2} - \frac{1}{3}e^{\imath\omega\triangle x}) \\ &= \frac{c}{\Delta x}((-\frac{1}{6}\cos(2\omega\triangle x) + \frac{2}{3}\cos(\omega\triangle x) - \frac{1}{2}) + (\frac{1}{6}\sin(2\omega\triangle x) - \frac{4}{3}\sin(\omega\triangle x))\imath)\hat{u}(\omega,t)\end{aligned} \tag{3.21}$$

Compared with $F(t,u) = su$, we have

$$s = \frac{c}{\Delta x}((-\frac{1}{6}\cos(2\omega\triangle x) + \frac{2}{3}\cos(\omega\triangle x) - \frac{1}{2}) + (\frac{1}{6}\sin(2\omega\triangle x) - \frac{4}{3}\sin(\omega\triangle x))\imath)$$

and we get

$$\begin{aligned}\mu &= \frac{c\Delta t}{\Delta x}((-\frac{1}{6}\cos(2\omega\triangle x) + \frac{2}{3}\cos(\omega\triangle x) - \frac{1}{2}) + (\frac{1}{6}\sin(2\omega\triangle x) - \frac{4}{3}\sin(\omega\triangle x))\imath) \\ &= \lambda_{cfl}((-\frac{1}{6}\cos(2\omega\triangle x) + \frac{2}{3}\cos(\omega\triangle x) - \frac{1}{2}) + (\frac{1}{6}\sin(2\omega\triangle x) - \frac{4}{3}\sin(\omega\triangle x))\imath)\end{aligned} \tag{3.22}$$

In order to get stability, μ in (3.22) should satisfy (3.20). By solving the inequality one can get a range of λ_{cfl}. The maximum value of this range is recorded as $(\lambda_{cfl})_{\max}$. Because of the algebraic complexity, it is usually difficult to obtain analytically the value $(\lambda_{cfl})_{\max}$. Instead, a procedure in Matlab can be used to get $(\lambda_{cfl})_{\max}$ numerically. The values of $(\lambda_{cfl})_{\max}$ of the different upwind-biased schemes considered in this paper are listed in Table 3.1.

Table 3.1: $(\lambda_{cfl})_{\max}$ of different schemes

Scheme	$(\lambda_{cfl})_{max}$
Third order scheme	1.62
Fifth order scheme	1.43
Seventh order scheme	1.24
Ninth order scheme	1.12
Eleventh order scheme	1.04
Thirteenth order scheme	0.99

3.2.1 GKS analysis

For GKS analysis, $\tilde{s}$ is the eigenvalue obtained in the semi-discrete case and

$$\mu = s\Delta t = (\lambda_{cfl})_{\max}\tilde{s}$$

There may exist more than one eigenvalues $\tilde{s}$, the maximum value of $|z|$ is shown in Figure 3.4 by the software Mathematica.

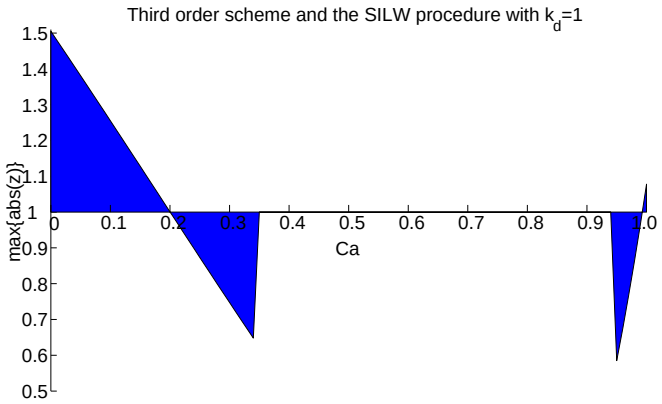

Figure 3.4: GKS analysis: third order scheme and the SILW procedure with $k_d = 1$

3.2.2 Eigenvalue spectrum visualization

This method is based on the matrix formulation (3.18). After discretizing in time with the third order Runge-Kutta method, we can get

$$\vec{U}^{n+1} = (I + (-\frac{c\Delta t}{\Delta x}Q) + \frac{1}{2}(-\frac{c\Delta t}{\Delta x}Q)^2 + \frac{1}{6}(-\frac{c\Delta t}{\Delta x}Q)^3)\vec{U}^n \tag{3.23}$$

where I is the identity matrix.

Making use of the analysis of the fully-discrete scheme before, we assume a solution of the form $\vec{U}^n = z^n\vec{U}^0$. Substituting this solution into (3.23), we can get

$$z\vec{U}^n = G\vec{U}^n$$
$$G = I - \frac{c\Delta t}{\Delta x}Q + \frac{1}{2}(\frac{c\Delta t}{\Delta x}Q)^2 - \frac{1}{6}(\frac{c\Delta t}{\Delta x}Q)^3$$

where z can be recognized as an eigenvalue with $\vec{U}^n$ as the associated eigenvector of the matrix G. If such eigenvalue with $|z| > 1$ with an associated non-trivial eigenvector exists, the scheme is unstable. That is, we need all the eigenvalues of G to lie inside the unit circle. i.e. $|z| \leq 1$, to ensure stability of the fully-discrete approximation.

Result of this analysis for the third order scheme and the SILW procedure with $k_d = 1$ is shown in Figure 3.5.

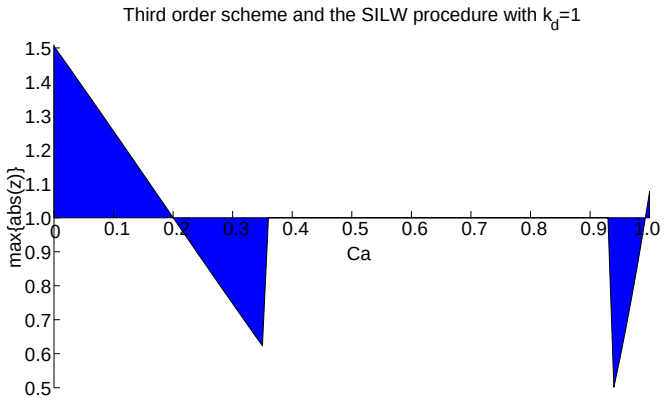

Figure 3.5: Eigenvalue spectrum analysis: Third order scheme and the SILW procedure with $k_d = 1$.

One can see that Figure 3.4 and Figure 3.5 are almost the same, indicating that both

methods of analysis produce consistent results. The scheme is not stable when C_a is small.

If we use procedures in Section 3.2.1 and Section 3.2.2 to the third order scheme and the SILW procedure with $k_d = 2$, there exists no eigensolution, indicating that the scheme is stable for all C_a.

Next, in Table 3.2, we give the results of the stability analysis, giving $(k_d)_{\min}$ required for the SILW inflow boundary treatment for different schemes to remain stable, under the same $(\lambda_{cfl})_{\max}$ as shown in Table 3.1 for pure initial value problems. Again, the third order TVD Runge-Kutta method is used for the time discretization.

Table 3.2: $(k_d)_{\min}$ to ensure stability for schemes of different orders

Scheme	$(k_d)_{\min}$
Third order scheme	2
Fifth order scheme	3
Seventh order scheme	4
Ninth order scheme	6
Eleventh order scheme	8
Thirteenth order scheme	10

For the remaining schemes in Section 2.1, results as in Figure 3.5 are shown in Figures 3.6, 3.7 and 3.8. These figures indicate the value ranges of C_a for which the scheme is unstable with k_d just below the stability thresholds listed in Table 3.2.

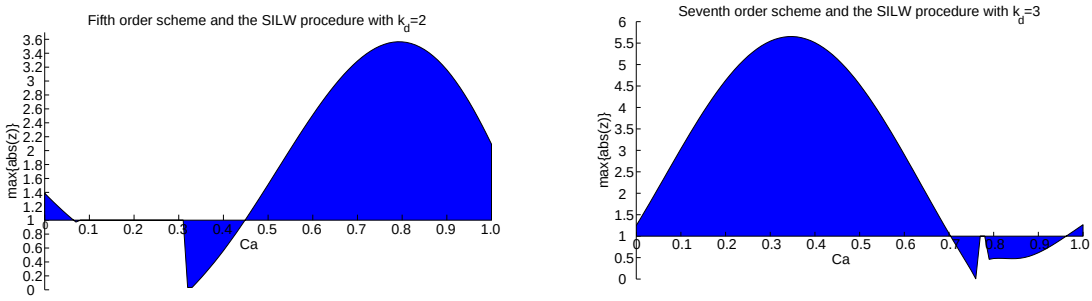

Figure 3.6: Results of the fifth order scheme and the SILW procedure with $k_d = 2$ (left) and the seventh order scheme and the SILW procedure with $k_d = 3$ (right).

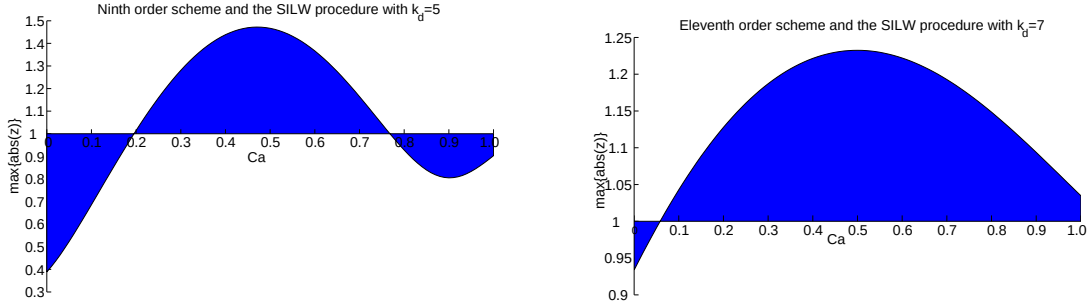

Figure 3.7: Results of the ninth order scheme and the SILW procedure with $k_d = 5$ (left) and the eleventh order scheme and the SILW procedure with $k_d = 7$ (right).

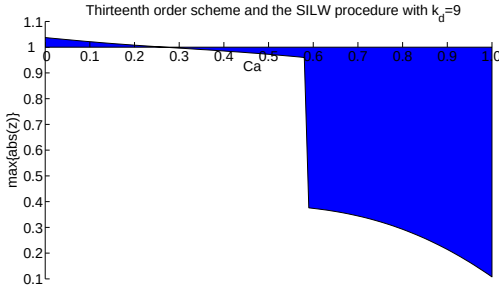

Figure 3.8: Results of the thirteenth order scheme and the SILW procedure with $k_d = 9$.

4 Numerical examples

In this section we provide numerical examples to demonstrate the stability results predicted by the analysis in Table 3.2.

4.1 The linear advection equation

The first example is an one-dimensional linear advection equation

$$\begin{cases} u_t + u_x = 0, \ x \in [-1, 1], \ t \geq 0 \\ u(-1, t) = g(t) = 0.25 + 0.5 \sin(\pi t), \ t \geq 0 \\ u(x, 0) = 0.25 + 0.5 \sin(\pi x), \ x \in [-1, 1] \end{cases} \tag{4.24}$$

The exact solution is

$$u(x, t) = 0.25 + 0.5 \sin(\pi(x - t))$$

In order to verify stability, we choose

$$\Delta t = (\lambda_{cfl})_{\max} \Delta x \tag{4.25}$$

• Third order scheme.

We first consider the third order scheme and the SILW procedure with $k_d = 1$. We choose $C_a = 0.001$, i.e. the physical inflow boundary is very close to the first grid point, a typical situation of "cut cells". Figure 4.9 (left) shows that the solution has strong spurious oscillations with very large magnitudes after a short computational time. This clearly demonstrate that the method is unstable, which is consistent with the analysis. When we take $k_d = 2$, as shown in Figure 4.9 (right), the solution remains stable and accurate after a very long time simulation, clearly demonstrating the stability of the scheme predicted by theory. A grid refinement study (not shown here to save space) verifies the designed third order accuracy.

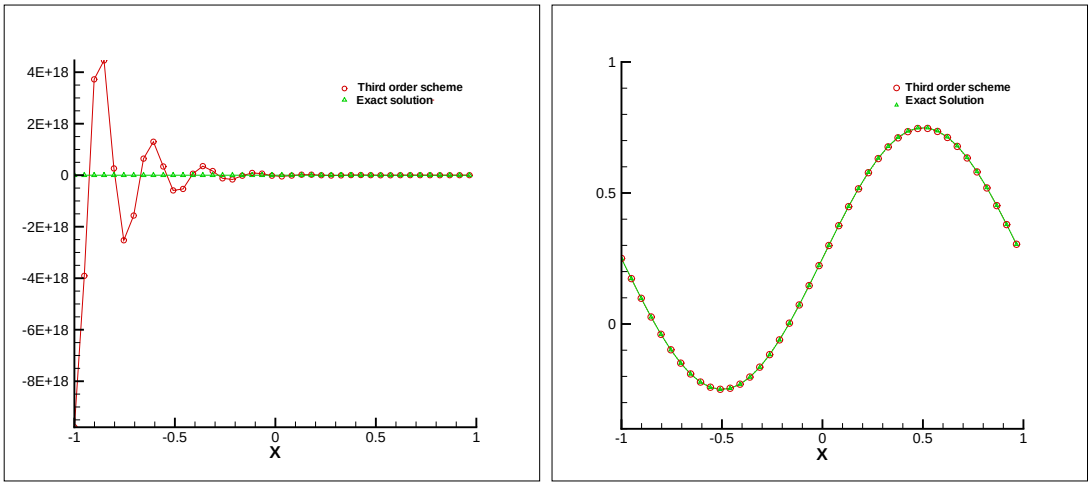

Figure 4.9: Numerical results obtained with the third order scheme. $C_a = 0.001$, $C_b = 0.7$ with $N = 40$ grid points. Left: $k_d = 1$, $t = 10$; Right: $k_d = 2$, $t = 10000$.

- Fifth order scheme.

Next, we consider the fifth order scheme and the SILW procedure with $k_d = 2$. Figure 4.10 (left) shows that the solution has strong spurious oscillations with very large magnitudes after a short computational time. This clearly demonstrate that the method is unstable, which is consistent with the analysis. When we take $k_d = 3$, as shown in Figure 4.10 (right), the solution remains stable and accurate after a very long time simulation, clearly demonstrating the stability of the scheme predicted by theory. Again, the result of a grid refinement study to verify accuracy is not shown to save space.

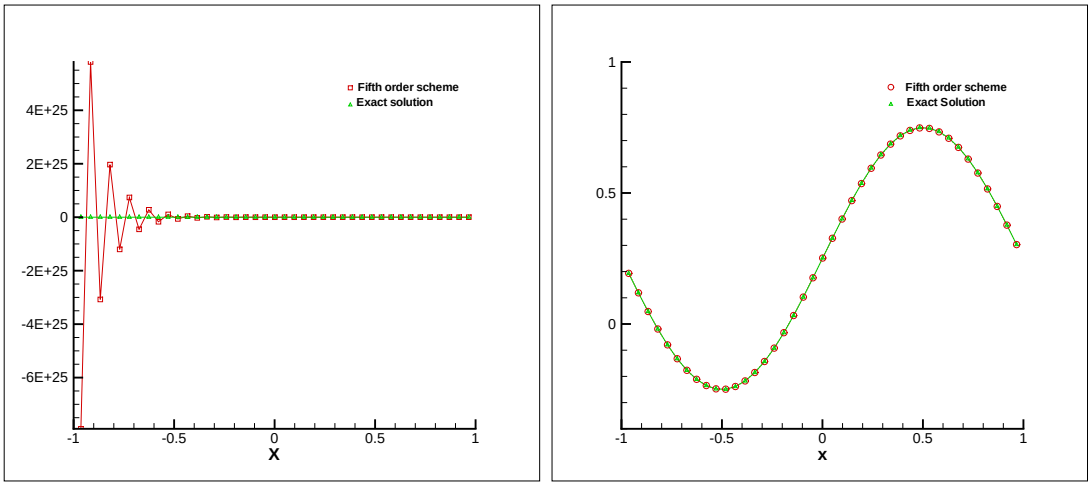

Figure 4.10: Numerical results obtained with the fifth order scheme. $C_a = 0.75$, $C_b = 0.7$ with $N = 40$ grid points. Left: $k_d = 2$, $t = 4$; Right: $k_d = 3$, $t = 10000$.

- Seventh order scheme.

We repeat our numerical experiment with the seventh order scheme. With $k_d = 3$, Figure 4.11 (left) clearly shows instability. When we increase the terms using the ILW procedure to $k_d = 4$, the scheme becomes stable as shown in Figure 4.11 (right), which is consistent with the analysis.

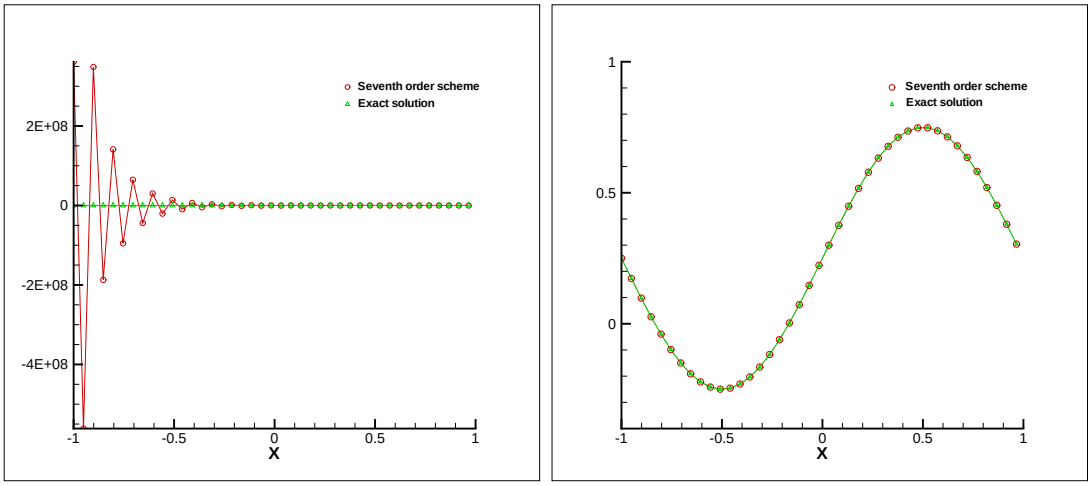

Figure 4.11: Numerical results obtained with the seventh order scheme. $C_a = 0.001$, $C_b = 0.7$ with $N = 40$ grid points. Left: $k_d = 3$, $t = 10$; Right: $k_d = 4$, $t = 10000$.

- Ninth order scheme.

The simulation for the ninth order scheme again verifies our analysis. Figure 4.12 (left) shows instability with $k_d = 5$, and Figure 4.12 (right) shows stability with $k_d = 6$.

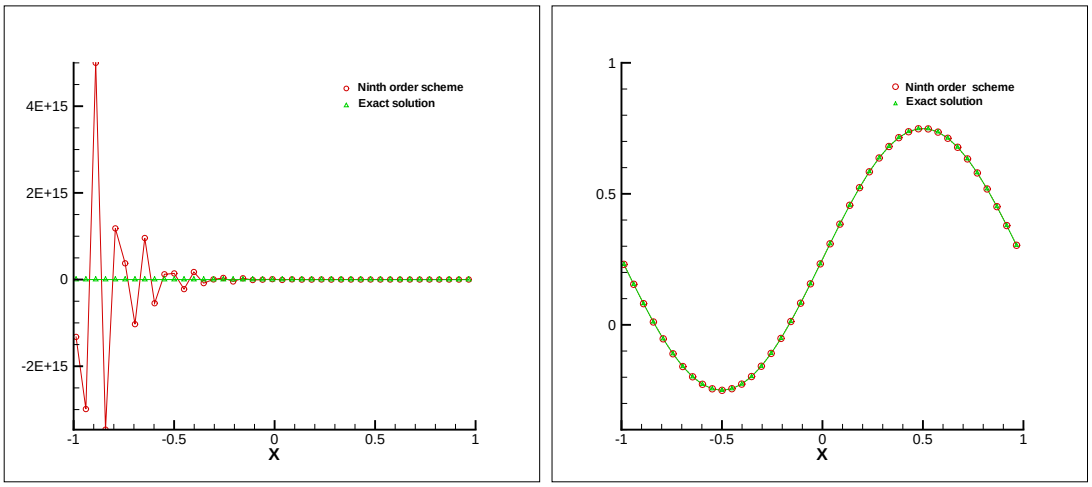

Figure 4.12: Numerical results obtained with the ninth order scheme. $C_a = 0.25$, $C_b = 0.7$ with $N = 40$ grid points. Left: $k_d = 5$, $t = 20$; Right: $k_d = 6$, $t = 10000$.

- Eleventh order scheme.

The simulation is repeated for the eleventh order scheme with $k_d = 7$ (Figure 4.13 left) showing instability and with $k_d = 8$ (Figure 4.13 right) showing stability.

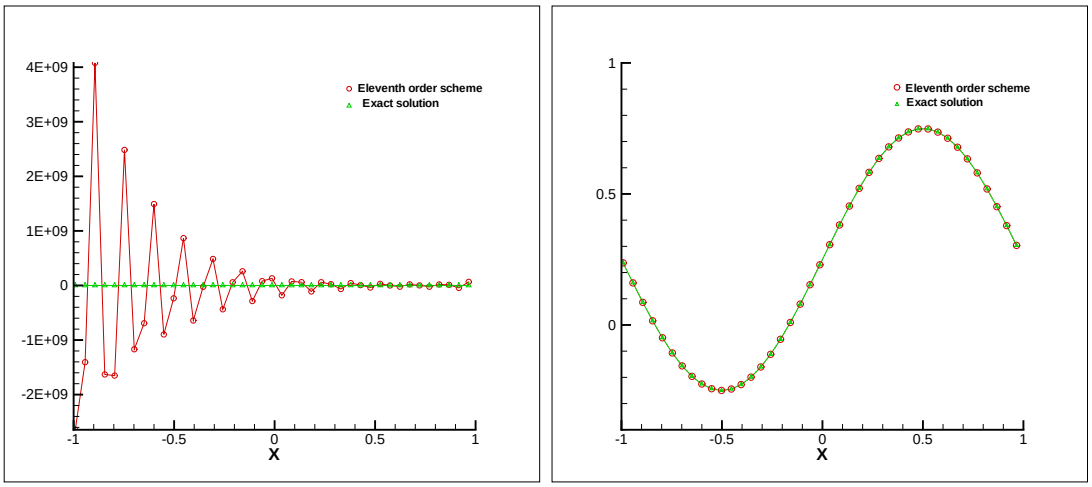

Figure 4.13: Numerical results obtained with the eleventh order scheme. $C_a = 0.17$, $C_b = 0.7$ with $N = 40$ grid points. Left: $k_d = 7$, $t = 20$; Right: $k_d = 8$, $t = 10000$.

- Thirteenth order scheme

Finally, the simulation is performed for the thirteenth order scheme with $k_d = 9$ (Figure 4.14 left) showing instability and with $k_d = 10$ (Figure 4.14 right) showing stability.

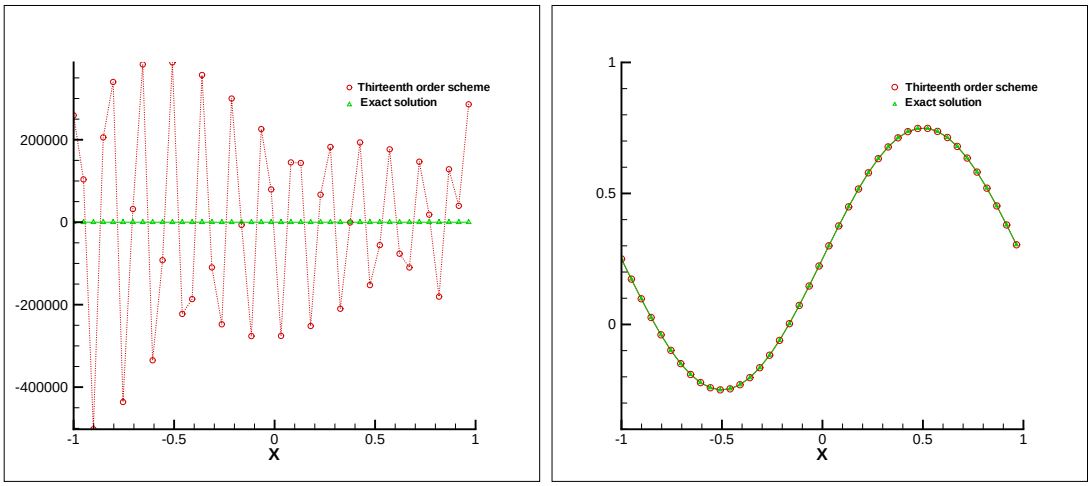

Figure 4.14: Numerical results obtained with the thirteenth order scheme. $C_a = 0.001$, $C_b = 0.7$ with $N = 40$ grid points. Left: $k_d = 9$, $t = 40$; Right: $k_d = 10$, $t = 10000$.

4.2 Burgers equation

In this subsection we pay our attention to the nonlinear scalar Burgers equation

$$\begin{cases} u_t + (\frac{u^2}{2})_x = 0, \ x \in [0, 2\pi], \ t \geq 0 \\ u(0,t) = g(t), \ t \geq 0 \\ u(x,0) = u_0(x), \ x \in [0, 2\pi] \end{cases} \tag{4.26}$$

where $u_0(x)$ is the initial condition. We assume $u(0,t) > 0$, hence $x = 0$ is an inflow boundary and $g(t)$ is the prescribed boundary condition. We take $g(t) = \hat{u}(0,t)$, where $\hat{u}(x,t)$ is the exact solution of the initial value problem on $(0, 2\pi)$ with periodic boundary condition for all t.

Two examples are given in this section. For simplicity, we will only test the third order scheme and the fifth order scheme as the inner schemes.

4.2.1 Example 1

We take the initial condition as

$$u_0(x) = 1 + 0.5\ \sin(x) \tag{4.27}$$

At $t = 1.0$, we have a smooth solution. Values of the ghost points near the inflow boundary are obtained by the SILW method. When considering ghost points near the outflow boundary, we use extrapolation in the appropriate order. From the previous analysis, if we use the fifth order scheme to approximate the spatial derivative, we need $k_d = 3$ in the SILW procedure to ensure stability for all values of C_a. In this example, it appears that $k_d = 2$ is enough to ensure stability for all values of C_a. The numerical results are summarized in Tables 4.3 and 4.4.

Firstly, we use

$$\Delta t = \frac{\lambda_{cfl}\,\Delta x}{\alpha} \tag{4.28}$$

to verify stability.

Secondly, we use

$$\Delta t = \frac{\lambda_{cfl}\,(\Delta x)^{\frac{5}{3}}}{\alpha} \tag{4.29}$$

to verify the designed order of accuracy.

In numerical examples, we always set $\lambda_{cfl} = (\lambda_{cfl})_{\max}$, and $\alpha = \max\limits_{0\le i\le N}\{|u_i^n|\}$ where u_i^n is the numerical solution at time level n and grid x_i.

Table 4.3 shows that the fifth order scheme using the SILW procedure with $k_d = 2$ is stable for this example, under the maximum CFL number for the inner scheme, for $C_a = 0.75$ and $C_a = 0.40$. Of course, only third order accuracy can be obtained asymptotically, restricted by the time discretization accuracy. Even though we do not list the results, stability has also been observed with $k_d = 2$ for other values of C_a. This appears to be better than what our analysis indicates before, which would predict that $k_d = 3$ is needed for stability over the whole range of C_a. Besides nonlinearity, the main reason might be that the solution varies quite a lot over the computational domain, and the

Table 4.3: Fifth order scheme with $k_d = 2$, $C_b = 0.7$ at $t = 1.0$ for (4.27) with (4.28)

N	$C_a = 0.75$				$C_a = 0.40$			
	L^2 *error*	order	L^∞ *error*	order	L^2 *error*	order	L^∞ *error*	order
40	1.481E-03	–	1.892E-03	–	1.461E-03	–	1.871E-03	–
80	2.069E-04	2.839	3.054E-04	2.631	2.100E-04	2.799	3.134E-04	2.578
160	2.892E-05	2.839	4.598E-05	2.732	2.878E-05	2.867	4.577E-05	2.776
320	3.632E-06	2.993	5.841E-06	2.977	3.643E-06	2.982	5.865E-06	2.964
640	4.656E-07	2.964	7.569E-07	2.948	4.669E-07	2.964	7.596E-07	2.949
1280	5.837E-08	2.996	9.507E-08	2.993	5.834E-08	3.001	9.500E-08	2.999

solution near the inflow boundary $x = 0$, which is of the size $\max_{0\le t\le 1} |g(t)|$, is much less than $\alpha = \max |u^n|$. Hence the effective CFL limit near the boundary $x = 0$ is less than $(\lambda_{cfl})_{\max}$. Even though we have shown before that, under the maximum CFL condition for the inner scheme $\lambda_{cfl} = 1.43$, we would need $k_d = 3$ to ensure stability for the whole range of C_a, we can also show that, if we allow a smaller CFL number $\lambda_{cfl} \le 1.02$, then $k_d = 2$ is enough to ensure stability for the whole range of C_a. We can verify that, under the time step restriction (4.28), $\max_{0\le t\le 1} |g(t)| \frac{\Delta t}{\Delta x}$ is indeed less than 1.02. Hence the numerical stability in this case is not surprising. This example shows that sometimes stability is better for nonlinear problems than for linear problems.

Clearly, if we use the time step (4.29), we can observe the designed fifth order of accuracy in Table 4.4.

4.2.2 Example 2

We now consider a different initial condition

$$u_0(x) = 1 + 0.2 \ \sin(x) \tag{4.30}$$

The difference from the previous initial condition is that $|u^n|$ does not vary as much when comparing its value near the inflow boundary $x = 0$ and over the whole computational

Table 4.4: Fifth order scheme with $k_d = 2$, $C_b = 0.7$ at $t = 1.0$ for (4.27) with (4.29)

N	$C_a = 0.75$				$C_a = 0.40$			
	L^2 *error*	order	L^∞ *error*	order	L^2 *error*	order	L^∞ *error*	order
40	2.430E-04	–	3.925E-04	–	2.523E-04	–	3.862E-04	–
80	1.096E-05	4.470	2.313E-05	4.085	1.118E-05	4.495	2.318E-05	4.058
160	3.866E-07	4.826	8.304E-07	4.800	3.908E-07	4.839	8.457E-07	4.777
320	1.262E-08	4.937	2.752E-08	4.915	1.269E-08	4.944	2.773E-08	4.931
640	4.016E-10	4.974	8.787E-10	4.969	4.027E-10	4.978	8.816E-10	4.975
1280	1.265E-11	4.989	2.770E-11	4.987	1.267E-11	4.991	2.774E-11	4.990

domain.

- Third order scheme

Firstly, we use the SILW procedure with $k_d = 1$. We set the final time $t = 1$ and $C_a = 0.001$, and observe that errors in this case become lager as Δx is decreased, implying numerical instability. Next we take $k_d = 2$ and show the results in Table 4.5. We can clearly see that the scheme is stable in this case and the designed third order accuracy is obtained.

Table 4.5: Third order scheme with $k_d = 2$, $C_b = 0.7$ at $t = 1.0$ for (4.30) with (4.28)

N	$C_a = 0.001$				$C_a = 0.35$			
	L^2 *error*	order	L^∞ *error*	order	L^2 *error*	order	L^∞ *error*	order
40	4.616E-04	–	4.084E-04	–	4.733E-04	–	4.042E-04	–
80	6.423E-05	2.845	5.805E-05	2.815	6.573E-05	2.848	5.721E-05	2.821
160	8.589E-06	2.903	7.812E-06	2.893	8.884E-06	2.887	7.801E-06	2.874
320	1.087E-06	2.982	9.901E-07	2.980	1.124E-06	2.982	9.883E-07	2.981
640	1.373E-07	2.985	1.252E-07	2.983	1.421E-07	2.984	1.250E-07	2.983
1280	1.730E-08	2.988	1.579E-08	2.987	1.792E-08	2.987	1.578E-08	2.985

• Fifth order scheme

Firstly, we use the SILW procedure with $k_d = 2$. We choose $t = 1$, and $C_a = 0.75$, and observe that the errors become lager as Δx is decreased when the time step is taken according to (4.28), indicating instability. Next, we increase k_d to $k_d = 3$. Stable and accurate results are then obtained, summarized in Tables 4.6 and 4.7 for the time steps taken according to (4.28) and (4.29) respectively.

Table 4.6: Fifth order scheme with $k_d = 3$, $C_b = 0.7$ at $t = 1.0$ for (4.30) with (4.28)

N	$C_a = 0.75$				$C_a = 0.40$			
	L^2 *error*	order	L^∞ *error*	order	L^2 *error*	order	L^∞ *error*	order
40	2.212E-04	–	2.004E-04	–	2.283E-04	–	2.047E-04	–
80	3.156E-05	2.809	2.905E-05	2.786	3.173E-05	2.847	2.918E-05	2.810
160	4.084E-06	2.950	3.778E-06	2.943	4.117E-06	2.946	3.806E-06	2.939
320	5.293E-07	2.948	4.903E-07	2.946	5.296E-07	2.958	4.906E-07	2.955
640	6.653E-08	2.992	6.169E-08	2.990	6.664E-08	2.991	6.179E-08	2.989
1280	8.394E-09	2.987	7.787E-09	2.986	8.404E-09	2.987	7.796E-09	2.987

Table 4.7: Fifth order scheme with $k_d = 3$, $C_b = 0.7$ at $t = 1.0$ for (4.30) with (4.29)

N	$C_a = 0.75$				$C_a = 0.40$			
	L^2 *error*	order	L^∞ *error*	order	L^2 *error*	order	L^∞ *error*	order
40	8.062E-06	–	7.695E-06	–	8.466E-06	–	8.151E-06	–
80	2.921E-07	4.786	2.887E-07	4.736	2.956E-07	4.840	2.936E-07	4.795
160	9.674E-09	4.916	9.634E-09	4.905	9.760E-09	4.921	9.749E-09	4.913
320	3.114E-10	4.957	3.106E-10	4.955	3.119E-10	4.968	3.123E-10	4.964
640	9.869E-12	4.980	9.852E-12	4.978	9.858E-12	4.984	9.879E-12	4.982
1280	3.095E-13	4.995	3.119E-13	4.981	3.081E-13	5.000	3.129E-13	4.981

4.3 Euler equations

The analysis performed in this paper can be easily generalized to linear hyperbolic systems. The numerical procedure works well also for nonlinear hyperbolic conservation laws, such as Euler equations of compressible gas dynamics

$$\vec{U}_t + \vec{F}(\vec{U})_x = 0,\ x \in [a,b],\ t > 0 \tag{4.31}$$

where the conservative variables are given by

$$\vec{U} = \begin{pmatrix} u_1 \\ u_2 \\ u_3 \end{pmatrix} = \begin{pmatrix} \rho \\ \rho u \\ E \end{pmatrix}$$

and the flux is given by

$$\vec{F}(\vec{U}) = \begin{pmatrix} u_2 \\ (\gamma-1)u_3 + \frac{3-\gamma}{2}\frac{u_2^2}{u_1} \\ (\gamma u_3 - \frac{\gamma-1}{2}\frac{u_2^2}{u_1})\frac{u_2}{u_1} \end{pmatrix}$$

where ρ is density, u is velocity, $E = \frac{1}{2}\rho u^2 + \rho e$ represents the total energy and p is the pressure. The equation of state is $e = \frac{p}{(\gamma-1)\rho}$. Here we choose $\gamma = 1.4$.

We take $a = -\pi$ and $b = \pi$ in (4.31) and the initial condition

$$\begin{cases} \rho_0(x) = 1 + 0.2\ \sin(x),\ x \in [-\pi,\pi],\ t \geq 0 \\ u_0(x) = 2,\ x \in [-\pi,\pi] \\ p_0(x) = 2,\ x \in [-\pi,\pi] \end{cases}$$

The exact solution with periodic boundary condition is

$$\begin{cases} \rho(x,t) = 1 + 0.2\ \sin(x-2t),\ x \in [-\pi,\pi],\ t \geq 0 \\ u(x,t) = 2,\ x \in [-\pi,\pi],\ t \geq 0 \\ p(x,t) = 2,\ x \in [-\pi,\pi],\ t \geq 0 \end{cases}$$

The three eigenvalues of the Jacobian matrix $\vec{F}'(\vec{U})$ are $u-c,\ u,\ u+c$ where $c=\sqrt{\frac{\gamma p}{\rho}}$ is the sound speed. Since $c<2=u$, the three eigenvalues are all greater than 0 in the whole domain $(x,t)\in[-\pi,\pi]\times[0,+\infty)$. $x=-\pi$ is an inflow boundary and $x=\pi$ is an outflow boundary for the three variables. The boundary condition for the inflow boundary in the conservative variables is

$$\begin{cases} u_1(-\pi,t) = g_1(t) = 1+0.2\ \sin(2t),\ t\geq 0 \\ u_2(-\pi,t) = g_2(t) = 2+0.4\ \sin(2t),\ t\geq 0 \\ u_3(-\pi,t) = g_3(t) = 2+0.4\ \sin(2t)+\dfrac{2}{\gamma-1},\ t\geq 0 \end{cases}$$

The details of the ILW and SILW procedures for hyperbolic systems are obtained along the same lines as those for the scalar equations, but are algebraically more complicated. We omit the derivation details here to save space and refer to [16, 18]. We use the third order scheme and the fifth order scheme to solve (4.31).

• Third order scheme

Firstly, we use SILW procedure with $k_d=1$. We choose $t=1$ and $C_a=0.001$, and observe that the errors become lager as Δx decreases, indicating instability. Results of the third order scheme and the SILW procedure with $k_d=2$ are stable and accurate, and are given in Table 4.8.

Table 4.8: Third order scheme with $k_d=2$, $C_b=0.7$ at $t=1.0$ for (4.31) with (4.28).

N	$C_a=0.001$				$C_a=0.35$			
	L^2 *error*	order	L^∞ *error*	order	L^2 *error*	order	L^∞ *error*	order
40	2.223E-04	–	1.919E-04	–	2.763E-04	–	1.869E-04	–
80	2.860E-05	2.958	2.447E-05	2.971	3.616E-05	2.934	2.417E-05	2.952
160	3.646E-06	2.972	3.085E-06	2.988	4.622E-06	2.968	3.064E-06	2.980
320	4.601E-07	2.986	3.866E-07	2.996	5.841E-07	2.984	3.854E-07	2.991
640	5.778E-08	2.993	4.837E-08	2.999	7.339E-08	2.993	4.830E-08	2.996
1280	7.245E-09	2.996	6.052E-09	2.999	9.200E-09	2.996	6.046E-09	2.998

• Fifth order scheme

Firstly, we use the SILW procedure with $k_d = 2$. We choose $t = 1$ and $C_a = 0.75$, and observe that the errors become lager as Δx decreases, implying instability.

Results of the fifth order scheme and the SILW procedure with $k_d = 3$, under two different choices of time steps, are given in Tables 4.9 and 4.10 respectively. Table 4.9 shows that the fifth order scheme and the SILW procedure with $k_d = 3$ is stable under the maximum allowable CFL number for the inner scheme. Table 4.10 shows the designed fifth order of accuracy when smaller time steps are taken.

Table 4.9: Fifth order scheme with $k_d = 3$, $C_b = 0.7$ at $t = 1.0$ for (4.31) with (4.28).

N	$C_a = 0.75$				$C_a = 0.40$			
	L^2 *error*	order	L^∞ *error*	order	L^2 *error*	order	L^∞ *error*	order
40	3.454E-05	–	2.351E-05	–	3.497E-05	–	2.390E-05	–
80	4.544E-06	2.926	3.096E-06	2.924	4.593E-06	2.928	3.130E-06	2.933
160	5.772E-07	2.977	3.942E-07	2.974	5.821E-07	2.980	3.972E-07	2.978
320	7.325E-08	2.978	5.007E-08	2.977	7.359E-08	2.984	5.027E-08	2.982
640	9.230E-09	2.988	6.311E-09	2.988	9.253E-09	2.992	6.325E-09	2.991
1280	1.159E-09	2.994	7.923E-10	2.994	1.159E-09	2.997	7.928E-10	2.996

Table 4.10: Fifth order scheme with $k_d = 3$, $C_b = 0.7$ at $t = 1.0$ for (4.31) with (4.29).

N	$C_a = 0.75$				$C_a = 0.40$			
	L^2 *error*	order	L^∞ *error*	order	L^2 *error*	order	L^∞ *error*	order
40	1.564E-06	–	1.136E-06	–	1.811E-06	–	1.186E-06	–
80	5.397E-08	4.857	3.981E-08	4.835	5.904E-08	4.939	4.069E-08	4.865
160	1.777E-09	4.924	1.309E-09	4.927	1.898E-09	4.959	1.359E-09	4.904
320	5.701E-11	4.962	4.199E-11	4.962	6.023E-11	4.978	4.466E-11	4.928
640	1.811E-12	4.976	1.711E-12	4.617	1.665E-12	5.177	1.710E-12	4.707

5 Concluding remarks

In this paper, we have discussed stability of high order upwind-biased finite difference schemes for solving hyperbolic conservation laws on a finite domain. Values of ghost points near the inflow boundary are obtained by an inverse Lax-Wendroff (ILW) or a simplified ILW (SILW) procedure and values of ghost points near the outflow boundary are obtained by a classical Lagrangian extrapolation of appropriate order. The outflow extrapolation and inflow ILW boundary treatments have both been proved to maintain stability and the order of accuracy, with the same CFL number $(\lambda_{cfl})_{\max}$ as the periodic case, for any of the high order schemes presented and for any C_a, which measures the distance between the physical boundary and the closet grid point. For the SILW boundary treatment, stability depends on k_d, which is the number of terms obtained by the ILW procedure. SILW maintains stability with $(\lambda_{cfl})_{\max}$ as the periodic case for any C_a when k_d is at least taken as $(k_d)_{\min}$, whose values for various orders of schemes are summarized in Table 3.2 by our stability analysis. Numerical examples are provided to demonstrate stability or instability predicted by the analysis in Table 3.2. Stability analysis in this paper is performed based on both the GKS analysis and eigenvalue spectrum visualization. The GKS analysis breaks the problem into three simpler problems, the inner problem and the two quarter-plane problems corresponding to the two types of boundaries. It is mathematically rigorous but could be algebraically highly complicated, especially for high order schemes. The eigenvalue spectrum visualization method transforms the scheme into a matrix form, containing both boundary conditions. It can be relatively easily performed for high order methods. It appears that, when both methods are applied, they produce consistent prediction for stability. The results of this paper are expected to provide valuable guidance to users of high order upwind-biased finite difference schemes, such as WENO schemes, for solving hyperbolic problems with the SILW boundary treatment procedure. Even though the analysis is performed in one-dimension, the stability prediction is expected to be valid for multi-dimensional problems.

The SILW boundary treatment is particularly attractive for multi-dimensional problems with complex geometry of the computational domain, including moving geometry, when simulated by a finite difference method on a fixed Cartesian mesh, see [16, 17, 18] for numerical experiment examples.

References

[1] D.S. Balsara and C.-W. Shu, *Monotonicity preserving weighted essentially non-oscillatory schemes with increasingly high order of accuracy*, Journal of Computational Physics, 160:405–452, 2000.

[2] M.J. Berger, C. Helzel and R.J. Leveque, *h-box methods for the approximation of hyperbolic conservation laws on irregular grids*, SIAM Journal on Numerical Analysis, 41:893–918, 2003.

[3] M.H. Carpenter, D. Gottlieb, S. Abarbanel and W.-S. Don, *The theoretical accuracy of Runge-Kutta time discretizations for the initial boundary value problem: a study of the boundary error*. SIAM Journal on Scientific Computing, 16:1241-1252, 1995.

[4] M. Goldberg, *On a boundary extrapolation theorem by Kreiss*. Mathematics of Computation, 31:469-477, 1977.

[5] M. Goldberg and E. Tadmor, *Scheme-independent stability criteria for difference approximations of hyperbolic initial-boundary value problems. I*, Mathematics of Computation, 32:1097–1107, 1978.

[6] M. Goldberg and E. Tadmor, *Scheme-independent stability criteria for difference approximations of hyperbolic initial-boundary value problems. II*. Mathematics of Computation, 36:603–626, 1981.

[7] B. Gustafsson, H.-O. Kreiss and A. Sundström, *Stability theory of difference approximations for mixed initial boundary value problem. II*, Mathematics of Computation, 26:649–686, 1972.

[8] W.D. Henshaw, *A high-order accurate parallel solver for Maxwell's equations on overlapping grids*, SIAM Journal on Scientific Computing, 28:1730–1765, 2006.

[9] W.D. Henshaw, H.-O. Kreiss and L.G.M. Reyna, *A fourth-order accurate difference approximation for the incompressible Navier-Stokes equations*, Computers & Fluids, 23:575–593, 1994.

[10] L. Huang, C.-W. Shu and M. Zhang, *Numerical boundary conditions for the fast sweeping high order WENO methods for solving the Eikonal equation*, Journal of Computational Mathematics, 26:336–346, 2008.

[11] G. Jiang and C.-W. Shu, *Efficient implementation of weighted ENO schemes*. Journal of Computational Physics, 126:202-228, 1996.

[12] X.-D. Liu, S. Osher and T. Chan, *Weighted essentially nonoscillatory schemes*. Journal of Computational Physics, 115:200-212, 1994.

[13] C.-W. Shu, *High order weighted essentially nonoscillatory schemes for convection dominated problems*, SIAM Review, 51:82–126, 2009.

[14] C.-W. Shu and S. Osher, *Efficient implementation of essentially non-oscillatory shock-capturing schemes*. Journal of Computational Physics, 77:439-471, 1988.

[15] J.C. Strikwerda, *Initial boundary value problems for the method of lines*. Journal of Computational Physics, 34:94–107, 1980.

[16] S. Tan and C.-W. Shu, *Inverse Lax-Wendroff procedure for numerical boundary conditions of conservation laws*. Journal of Computational Physics, 229:8144–8166, 2010.

[17] S. Tan and C.-W. Shu, *A high order moving boundary treatment for compressible inviscid flows*, Journal of Computational Physics, 230:6023–6036, 2011.

[18] S. Tan, C. Wang, C.-W. Shu and J. Ning, *Efficient implementation of high order inverse Lax-Wendroff boundary treatment for conservation laws*. Journal of Computational Physics, 231:2510–2527, 2012.

[19] F. Vilar and C.-W. Shu, *Development and stability analysis of the inverse Lax-Wendroff boundary treatment for central compact schemes*. Mathematical Modelling and Numerical Analysis, 49:39–67, 2015.